Polariton propagation in weak-confinement quantum wells

D. Schiumarini, N. Tomassini, L. Pilozzi, and A. D'Andrea
Istituto dei Sistemi Complessi, CNR, CP 10, Monterotondo Stazione, Roma I-00016, Italy
(Received 31 March 2010; revised manuscript received 30 June 2010; published 3 August 2010)

Exciton-polariton propagation in a quantum well, under center-of-mass quantization, is computed by a variational self-consistent microscopic theory. The Wannier exciton envelope functions basis set is given by the simple analytical model of D'Andrea and Del Sole [Phys. Rev. B **41**, 1413 (1990)], based on pure states of the center-of-mass wave vector, free from fitting parameters and "*ad hoc*" (the so-called additional boundary conditions—ABCs) assumptions. In the present paper, the former analytical model is implemented in order to reproduce the center-of-mass quantization in a large range of quantum well thicknesses ($5a_B \leq L \leq \infty$). The role of the dynamical transition layer at the well/barrier interfaces is discussed at variance of the classical Pekar's dead layer and ABCs. The Wannier exciton eigenstates are computed and compared with various theoretical models with different degrees of accuracy. Exciton-polariton transmission spectra in large quantum wells ($L \gg a_B$) are computed and compared with experimental results of Schneider *et al.* [Phys. Rev. B **63**, 045202 (2001)] in high-quality GaAs samples. The sound agreement between theory and experiment allows to unambiguously assign the exciton-polariton dips of the transmission spectrum to the pure states of the Wannier exciton center-of-mass quantization.

DOI: 10.1103/PhysRevB.82.075303 PACS number(s): 78.67.De, 71.36.+c, 71.35.Cc

I. INTRODUCTION

Exciton-polariton propagation in mesoscopic superstructures has shown interesting physical phenomena. Superradiant effects in multi-quantum wells,[1–4] polariton propagation in uniaxial mesoscopic crystals,[5] soliton-polariton and shock waves propagation,[6] and polaritons condensation in distributed Bragg reflector (DBR) cavities[7] are present in the recent literature. All these phenomena are usually observed in exciton-polariton propagation experiments performed in optically nonlocal mesostructures. Among these, DBR microcavities and multi-quantum wells under Bragg condition are usually studied as paradigmatic systems showing strong radiation-matter interaction.[8–11] For instance, periodic N-quantum wells are usually well suited for studying superradiant exciton-polariton propagation that crucially depends on the optical properties of theirs $2N$ interfaces.[4,5] Moreover, if no overlapping between the exciton envelope functions, localized in adjacent quantum wells, are present, the so-called dead-layer model was largely used in order to describe the optical properties of the $2N$ interfaces of the system.[12–19] Recently, a large dead-layer effect was also observed in colloidal ZnO nano crystals and this surface optical passivation should be responsible on shorten the exciton lifetime in this kind of systems.[20]

In his pioneering paper,[21] Pekar introduced the concept of exciton "dead layer" (or extrinsic dead layer) in order to justify the three-layer model of the electric dipole polarization necessary to reproduce the reflectance line shape of Wannier exciton spectra in a semi-infinite semiconductor. In a subsequent paper,[22] Thomas and Hopfield discussed the microscopic basis (interface structural disorder, chemical disorder, image potential, impurities, etc.) of this classical effect. Looking forward a self-consistent microscopic computation of polariton propagation in semi-infinite samples in the semiclassical framework, D'Andrea and Del Sole[23] introduced an "intrinsic dead layer" (or transition layer) by imposing the minimization of the exciton envelope function mismatch at the vacuum/semiconductor surface, expanded in an hydrogenic basis set. In the same paper an analytical approximation of the semi-infinite exciton envelope function that exactly accomplishes the so-called no-escape boundary conditions (NEBCs) at surface plane ($Z=0$) of the sample, namely, $\Psi_K(z_e=0)=\Psi_K(z_h=0)=0$, was also given for computing the optical response at semiconductor band edge,[23,24]

$$\Psi_K(\vec{r},\vec{R}) = N_K[e^{-iKZ} + Ae^{iKZ} - (1+A)e^{-\bar{P}Z}]\varphi_{1s}(r)e^{i\vec{K}_\parallel\cdot\vec{R}_\parallel}/\sqrt{S}, \tag{1}$$

where $\vec{r}$ and $\vec{R}$ are the coordinates of the electron-hole (e-h) relative and center-of-mass motion, respectively, $\varphi_{1s}(r)$ is the $n=1$ hydrogenic wave function of the relative motion, K is the wave vector of the center-of-mass along Z axis (with $Z \geq 0$), $\vec{K}_\parallel$ is the corresponding in-plane wave vector, $A = -\frac{\bar{P}-iK}{\bar{P}+iK}$ is the exciton reflection amplitude on $Z=0$ vacuum/semiconductor surface ($|A|^2=1$), and $\bar{P}$ is an average coefficient of the evanescent waves due to the higher energy hydrogenic wave functions ($n>1$) taken close to the continuum states ($n \to \infty$).[23,24] Moreover the exciton energy is: $E_K = -R^*(a_B) + \frac{\hbar^2}{2M}[K^2+K_\parallel^2]$, where $R^*(a_B)$ is the three-dimensional (3D) Rydberg, M and μ are total and reduced mass, respectively, and a_B is the 3D Bohr radius of the exciton. The transition layer $1/\bar{P} = \delta_\infty$ is strongly dependent on the center-of-mass wave vector value K along Z axis[23] and coincides with the zone, close to the surface plane $Z=0$, where the exciton envelope function $\Psi_K(z_e;z_h;\vec{r}) \approx 0$.[23,24]

Notice that the transition layer of Eq. (1) is a quantum-mechanical quantity derived self-consistently by a variational principle, and due to the distortion of the exciton envelope function at surface, where center of mass and relative motion of the exciton are entangled, while Pekar's dead layer is a classical quantity characterizing the zone of the surface where the electric polarization is zero (additional boundary

condition—ABC) and due to the selvedge layer present in real samples.[22] Therefore, since Pekar's dead layer is usually determined as fitting parameter, its value can take into account not only the effect due to the boundary conditions imposed on the exciton envelope function (intrinsic dead layer) but also other physical effects present in real surfaces[22] (extrinsic dead layer).

The former analytical model of Eq. (1) was extended to the slab geometry[25] where the transition layer and the effective Bohr radius were determined by a variational minimization of the first momentum of the exciton Hamiltonian. Also in this case the average level was chosen close to the energy of the hydrogenic continuum states ($n \rightarrow \infty$).[25] Notice that the former choice, not strictly necessary for the consistency of the theory, induces some inconsistency as pointed out by the authors of Refs. 26 and 27. In the present paper a different choice, not affected by the former problem and that nicely reconciles[28] the transition layer in semi-infinite solids and in slabs, is suggested.

Exciton envelope functions in quantum confined systems (wells, wires, and dots) are usually computed by variational minimization of the exciton energy in a so-called "ABC free" theory.[29] Notice that in the large quantum well limit ($L \gg a_B$) a very accurate numerical minimization is necessary in order to determine a sensible dead-layer value. In fact, we remind that the interband transitions at semiconductor band edge are on the order of some electron volts in the visible range of energies and the Wannier exciton energies are close to the hydrogenic Rydberg: $R^*(a_B)=\frac{\hbar^2}{2\mu}\frac{1}{a_B^2}$ (on the order of tens of millielectron volt) while the center-of-mass energy of the exciton is given by: $E_{CM}(L \gg a_B) \approx \frac{\hbar^2}{2M}(\frac{\pi}{L})^2$ (on the order of tens of microelectron volt). Finally, the sensitiveness of the optical spectrum to the dead-layer effect can be given by the center-of-mass energy difference with and without the dead-layer effect, namely, $\Delta E(d)=E(L-2d)-E(L) \approx \frac{\hbar^2}{2M}(\frac{\pi}{L})^2\frac{4d}{L}$ (from about tens of microelectron volt to zero), where $\Delta E(d)/E(L) \approx 4d/L$. Therefore, many orders of magnitude[30] in the energy accuracy should be necessary for computing the Wannier exciton dynamics under the center-of-mass quantization.

Notice that the transition layer affects the exciton center-of-mass momentum (spatial dispersion effect) and gives additional light waves propagating into the sample, therefore its effect on the optical properties cannot be neglected neither in the presence of a large energy broadening. Even if it has a rather negligible effect on the energy position of exciton-polariton peaks in transmission spectra, we expect that it should have a non-negligible effect on the line-shape analysis and its role should be even enhanced in the time resolved optical spectra in multi-quantum well systems.[6,7]

The aim of the present work is twofolds: (i) a nonadiabatic Wannier exciton envelope function, obtained as a generalization of the analytical model of Ref. 25, is solved by a variational method, and compared with other model calculations at different degree of accuracy, namely, a more accurate variational expansion in e-h subband products,[31] an exact adiabatic solution,[27] and the heuristic so-called "hard-sphere" model. Notice that the former extension is necessary in order to study the limit of validity of the analytical model itself, and it becomes also mandatory when a complete one exciton basis set must be used, as in nonlinear optical computation.[32] (ii) In order to check the ability of the former analytical model in reproducing the exciton center-of-mass dynamics, the self-consistent optical transmission spectra in a single quantum well is computed and compared with experimental results of Schneider *et al.*[33] performed in high-quality GaAs quantum wells. A sound agreement is obtained for high-quality quantum wells both for intensity and phase measurements of the optical transmission spectrum with our analytical model for exciton masses ratio from the positronium limit ($\mu/M=0.248$) to the hydrogenic one ($\mu/M=0.111$); moreover, it allows to unambiguously assign the higher energy peaks, present in the spectrum of Ref. 33, to the pure states of the center-of-mass quantization.

In Sec. II the analytical Wannier exciton function model of Ref. 25 is revisited and generalized. We here remind all the approximations involved in order to facilitate the generalization of the analytical model at an order higher than the $1s$ hydrogenic wave function as explicitly reported in Appendix A. In Sec. III the optical response of a single quantum well is computed and compared with the experimental results of Schneider *et al.*[33]

II. WANNIER EXCITON IN A SLAB: VARIATIONAL ANALYTICAL MODEL REVISITED AND IMPLEMENTED

Let us consider a Wannier exciton of energy E, confined in a single quantum well of thickness $L \gg a_B$, and clad between two infinite potential barriers ($-L/2 \leq Z \leq L/2$). The exciton function, in a two-band model and in effective-mass approximation, can be expanded in a complete basis set of hydrogenic eigenstates:[25] $\hat{H}_{\vec{r}}\varphi_{nlm}(\vec{r})=\varepsilon_n\varphi_{nlm}(\vec{r})$, where $\hat{H}_{\vec{r}}=-\frac{\hbar^2}{2\mu}\vec{\nabla}^2_{\vec{r}}-\frac{e^2}{\varepsilon_b r}$,

$$\Psi_K(\vec{r},\vec{R}) = \Psi_E(\vec{r},Z)e^{i\vec{K}_\parallel\cdot\vec{R}_\parallel}/\sqrt{S}, \tag{2a}$$

$$\Psi_E(\vec{r},Z) = \sum_{nlm}[a_{nlm}e^{iK_nZ} + b_{nlm}e^{-iK_nZ}]\varphi_{nlm}(\vec{r}). \tag{2b}$$

The modulus of the exciton center-of-mass wave vector along Z axis is $K_n=\sqrt{K^2-K_\parallel^2}=\sqrt{[\frac{2M}{\hbar^2}(E-\varepsilon_n)]-K_\parallel^2}$, where $\vec{K}_\parallel$ is the wave vector along the (x,y) plane. Now, the sum on the hydrogenic basis set of Eq. (2) can be separated in a finite (for $E \geq \varepsilon_n+\hbar^2K_\parallel^2/2M$) and an infinite sum (with $E<\varepsilon_n+\hbar^2K_\parallel^2/2M$), that, at normal-incidence configuration ($K_\parallel=0.0$), give the following exciton envelope function:

$$\Psi_E(\vec{r},Z) = \sum_{nlm}^{\{E\geq\varepsilon_n\}}[\alpha_{nlm}\cos(K_nZ) + \beta_{nlm}\sin(K_nZ)]\varphi_{nlm}(\vec{r}) + \sum_{nlm}^{\{\varepsilon_n>E\}}[a_{nlm}e^{-P_nZ} + b_{nlm}e^{P_nZ}]\varphi_{nlm}(\vec{r}), \tag{3}$$

where $P_n=iK_n=[\frac{2M}{\hbar^2}(\varepsilon_n-E)]^{1/2}$ and $\alpha_{nlm}=a_{nlm}+b_{nlm}$, $\beta_{nlm}=i(a_{nlm}-b_{nlm})$.

The analytical approximation of the former wave function is obtained by adopting the procedure of Ref. 30. First of all,

we restrict the finite sum to only one hydrogenic function: the $1s$ $(n=1)$ state; the general case will be discussed in Appendix A and specialized for $n=2$.

The computation for a symmetric quantum well proceeds by defining the operator: $\hat{\mathbb{R}}(z\to -z; Z\to -Z)$ that, applied to the exciton envelope function of Eq. (3), gives the relationship: $\hat{\mathbb{R}}\Psi_E(\vec{r},Z)=\pm\Psi_E(\vec{r},Z)$. From this relation two sets of exciton envelope functions are generated for even and odd symmetries, respectively,

$$\Psi_E^e(\vec{r},Z)=\alpha_1\cos(K_1Z)\varphi_{1s}(r)+2\sum_{nlm}^{n>1}[\alpha_{nlm}\cosh(P_nZ)\varphi_{nlm}^e(\vec{r}) - \beta_{nlm}\sinh(P_nZ)\varphi_{nlm}^o(\vec{r})], \tag{4a}$$

$$\Psi_E^o(\vec{r},Z)=\beta_1\sin(K_1Z)\varphi_{1s}(r)+2\sum_{nlm}^{n>1}[\alpha_{nlm}\cosh(P_nZ)\varphi_{nlm}^o(\vec{r}) - \beta_{nlm}\sinh(P_nZ)\varphi_{nlm}^e(\vec{r})], \tag{4b}$$

where the coefficients α_1 and β_1 are $\alpha_1=\alpha_{100}$ and $\beta_1=\beta_{100}$.

In order to perform a smart truncation of the former series expansion, let us consider N-hydrogenic functions (with $N\to\infty$), and substitute the infinite sum of virtual states with an $(N-1)$ times degenerate state, located at an energy value much higher than E. Notice that the former approximation can be obtained by substituting $P_{n>1}$ with an average value $\bar{P}=1/\delta$, where δ is the transition layer of the Wannier exciton.[25] Therefore the former "one-transition layer" approximation of Wannier exciton envelope function is based on the substitution of the infinite sum of the hydrogenic basis set in Eqs. (4a) and (4b) with four analytical terminators that accomplish the NEBCs at the well/barrier interfaces. In fact, by imposing the NEBC: $\Psi_E(z_e=\pm L/2, z_h, \vec{\rho})=\Psi_E(z_h=\pm L/2, z_e, \vec{\rho})=0.0$ we can determine, as shown in Refs. 25 and 30, the following four rational functions:

$$F_{ee}(\vec{r})=2\sum_{nlm}^{n>1}(\alpha_{nlm}/\alpha_1)\varphi_{nlm}^e(\vec{r})=f_{ee}(z)\varphi_{1s}(r),$$

$$F_{oo}(\vec{r})=2\sum_{nlm}^{n>1}(\alpha_{nlm}/\alpha_1)\varphi_{nlm}^o(\vec{r})=f_{oo}(z)\varphi_{1s}(r),$$

$$F_{eo}(\vec{r})=2\sum_{nlm}^{n>1}(\beta_{nlm}/\beta_1)\varphi_{nlm}^o(\vec{r})=f_{eo}(z)\varphi_{1s}(r),$$

$$F_{oe}(\vec{r})=2\sum_{nlm}^{n>1}(\beta_{nlm}/\beta_1)\varphi_{nlm}^e(\vec{r})=f_{oe}(z)\varphi_{1s}(r)$$

that give the requested terminators as shown explicitly in Refs. 25 and 30 [and also in Appendix A see Eqs. (A5a), (A5b), (A6a), and (A6b)]. This approximation gives rather accurate numerical results when a large energy gap is present between the traveling $1s$ state and the virtual higher energy states, as will be carefully checked in the calculation and further discussed in this section. With the use of the former terminators the exciton envelope functions assume a compact analytical form,

$$\Psi_m^e(\vec{r},Z)=N_m^e[\cos(K_mZ)+\cosh(\bar{P}Z)f_{ee}^{(m)}(z)-\sinh(\bar{P}Z)f_{eo}^{(m)}\times(z)]\varphi_{1s}(r)$$

$$=N_m^e g_m^e(z,Z)\varphi_{1s}(r)\quad\text{for}\quad m=1,3,5,\ldots, \tag{5a}$$

$$\Psi_m^o(\vec{r},Z)=N_m^o[\sin(K_mZ)+\cosh(\bar{P}Z)f_{oo}^{(m)}(z)-\sinh(\bar{P}Z)f_{oe}^{(m)}\times(z)]\varphi_{1s}(r)$$

$$=N_m^o g_m^o(z,Z)\varphi_{1s}(r)\quad\text{for}\quad m=2,4,6,\ldots, \tag{5b}$$

where $K_m\equiv K_1(m)$ with m the center-of-mass quantum number for even and odd symmetries, and $\varphi_{1s}(r)=e^{-r/a}/\sqrt{\pi a^3}$ is the $1s$ hydrogenic function of the relative motion.

Finally, from the continuity of the exciton wave function $\Psi^{(i)}(z\to 0^+)=\Psi^{(i)}(z\to 0^-)$ and its first derivative $\frac{\partial\Psi^{(i)}}{\partial z}|_{z=0^+}=\frac{\partial\Psi^{(i)}}{\partial z}|_{z=0^-}$ for $i=e,o$ at $z=0$ surface of the relative motion, the relationships for the center-of-mass quantization are obtained. Notice that, due to the symmetry properties of the exciton envelope functions, the two former relations are reduced to the condition of approaching the z surface with zero first-order derivative, namely, $\frac{\partial F_{ee}}{\partial z}|_{z=0}=0$ and $\frac{\partial F_{oe}}{\partial z}|_{z=0}=0$. These conditions give the center-of-mass dispersion relations for even $(m=1,3,5,\ldots)$ and odd $(m=2,4,6,\ldots)$ excitons, respectively, namely,

$$K_m tg[K_mL/2]+\bar{P}tgh[\bar{P}L/2]=0\quad\text{for}\quad m=1,3,5,\ldots, \tag{6a}$$

$$\bar{P}tg[K_mL/2]-K_m tgh[\bar{P}L/2]=0\quad\text{for}\quad m=2,4,6,\ldots \tag{6b}$$

Obviously, the difference between the former quantization conditions and the simple condition $K_m=\frac{\pi}{L}m$ for $m=1,2,3,\ldots$ is due to the composed nature of the Wannier exciton and Eqs. (6a) and (6b) will recover the former simple condition in the limit value $m\to\infty$.

The variational minimization of the first momentum of the exciton Hamiltonian is computed for the lowest even and odd energy states $(m=1,2)$: $\langle\Psi_m|\hat{H}_{ex}|\Psi_m\rangle/\langle\Psi_m||\Psi_m\rangle=\min$, by taking as variational nonlinear parameters the effective Bohr radius (a) and the inverse of the transition layer $(\bar{P}=1/\delta)$. Even and odd variational parameters assume rather the same value for large quantum wells $(L\gg a_B)$ and exactly the same value in the bulk limit $(L\to\infty)$.[23,25]

Since the dynamics of an exciton, perfectly confined in a quantum well, strongly depends on the well thickness (L/a_B), let us consider the following different zones of quantum well dimensions, namely, (i) a zone of very large quantum wells $(L\gg a_B)$ or bulk limit $L\to\infty$, where both the variational parameters assume their bulk values, and therefore the exciton energy converges to the "hard-sphere model," namely, $E_m=-R^*(a_B)+m^2\frac{\hbar^2}{2M}(\frac{\pi}{L-2d})^2$ for $m=1,2,\ldots$ In this zone the transition layer assumes its saturation value $(\delta$

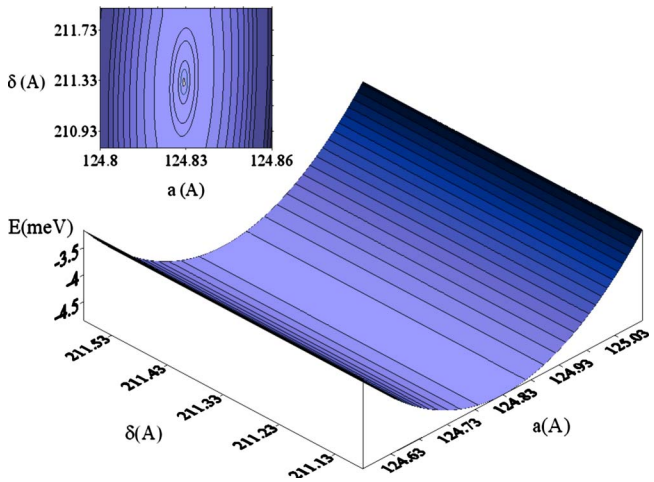

FIG. 1. (Color online) Exciton energy as a function of effective Bohr radius (a) and transition layer (δ) parameters in a AlGaAs/GaAs(001) quantum well of thickness $L=250$ nm. In the inset the minimum exciton energy is clearly shown.

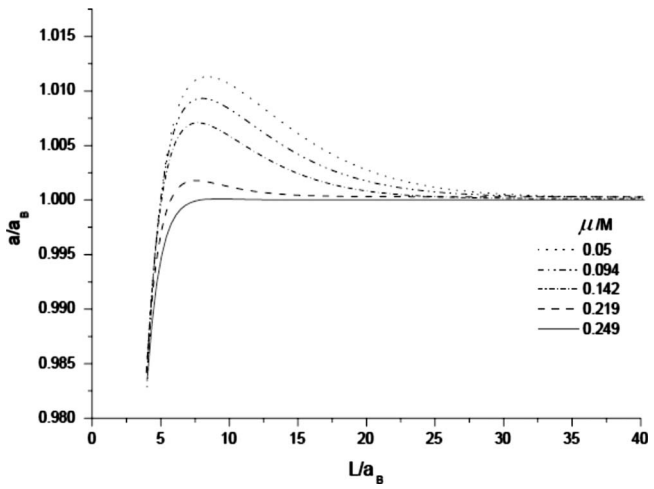

FIG. 2. Effective Bohr radius (a/a_B) as a function of quantum well thickness (L/a_B) computed for five different masses ratios (μ/M:0.050;0.094;0.142;0.219;0.249).

$=\delta_{L\to\infty}$) (Ref. 30) in numerical agreement with that obtained in a semi-infinite sample.[34,35] (ii) The center-of-mass quantization zone ($10a_B \leq L \leq 30a_B$), where the Bohr radius changes smoothly and its value remains rather close to the bulk one while the transition layer strongly depends on the quantum well thickness and dominates the exciton dynamics from hydrogenic ($\mu/M=0$) to positronium behavior ($\mu/M=1/4$). Notice that in this zone the former analytical model is well suited for describing the exciton composite dynamics. Moreover, (iii) by decreasing the quantum well thickness in the range $5a_B \leq L \leq 10a_B$ also the Bohr radius value shrinks. In this zone strong nonadiabatic effects, due to the entanglement between center-of-mass and relative motion, are present, and the analytic model could be implemented by higher energy hydrogenic wave function (see Appendix A). (iv) Finally, in the transition zone where Wannier exciton behavior changes from 3D→2D dynamics, the transition layer and the center-of-mass quantization along Z-axis loose their meanings.

In order to study the Wannier exciton behavior in the center-of-mass quantization the $m=1$ energy minimization is computed by adopting the formula reported in Ref. 30. In Fig. 1 the exciton energy, in a rather large AlGaAs/GaAs(001) quantum well, is shown as a function of the variational parameters value. The physical parameter values of the model are the same of Ref. 36, namely, $m_e=0.067m_o$, $m_{hh}=0.457m_o$, $n_b=3.71$, and $L=20a_B=250$ nm. In this system the heavy-hole Bohr radius and the Rydberg energy are $a_B=12.4649$ nm and $R^*(a_B)=-4.1965$ meV, respectively. Therefore, the Wannier exciton is in the center-of-mass quantization zone with a mass ratio $\mu/M=0.111$, rather close to the hydrogenic behavior.

Notice that in a scale where the minimum energy with respect to the effective Bohr radius is clearly shown, the one due to the transition layer is hardly observed (see the inset of Fig. 1).[37] Moreover, the minimized effective exciton radius is $a=12.4850\pm0.002$ nm and the transition layer $\delta=1/\bar{P}=21.160\pm0.002$ nm while the exciton energy for $m=1$ envelope function is $\varepsilon_1=-4.17975$ meV and the computed center-of-mass wave vector along Z axis is $K_{m=1}=0.795340\times10^{-3}$ a.u. The wave vector and the exciton energy, derived from the minimization, are both in rather good agreement with those computed by the hard-sphere model by taking the dead-layer value equal to the minimized transition layer ($d=\delta$). In fact, the hard-sphere model gives $\tilde{\varepsilon}_1=-R^*(a_B)+\hbar^2\tilde{K}_1^2/2M=-4.17985$ meV and $\tilde{K}_1=\pi/(L-2\delta)=0.800525\times10^{-3}$ a.u. while exciton wave vector computed by zero dead-layer value is strongly different ($\tilde{K}=\pi/L\approx0.665012\times10^{-3}$ a.u.) from both the former values.

Notice, from Eqs. (6a) and (6b), that the minimized transition layer of the analytical model coincides with the dead layer ($\delta=d$) for $m=1$ center-of-mass wave vector while increasing the m value ($m>1$) the dead-layer value decreases ($\delta>d$), till the limit value $m\to\infty$ where the center-of-mass wave vector is $K_m=m\pi/L$ in correspondence of negligible dead-layer value ($d\to0$) (see also Figs. 5 and 6).

In conclusion, the lowest energy exciton state ($m=1$) of our analytical model is in good agreement with the results obtained by the heuristic hard-sphere model when the dead layer is substituted by the corresponding minimized transition layer value. Moreover, the sound agreement with the "exact" adiabatic solution of Ref. 29 is fully discussed in Ref. 30 and will not be reported here again.

The transition layer of the nonadiabatic exciton envelope function of Eqs. (5a) and (5b) introduces an entanglement between relative and center-of-mass motion of the exciton that is the very reason that makes needless the ABC imposed to the Maxwell equations and that causes many electromagnetic waves propagation (spatial dispersion effect) also in semiconductor with cubic symmetry.[21,38]

A systematic analysis of the effective Bohr radius and of the transition layer as a function of the quantum well thickness, and for different values of the mass ratio μ/M are shown in Figs. 2 and 3, respectively. The dependence of the effective Bohr radius on the well thickness (Fig. 2) is a strong function of the mass ratio μ/M. In fact, it reaches its saturation limit at about $10a_B$ for positronium, while the hy-

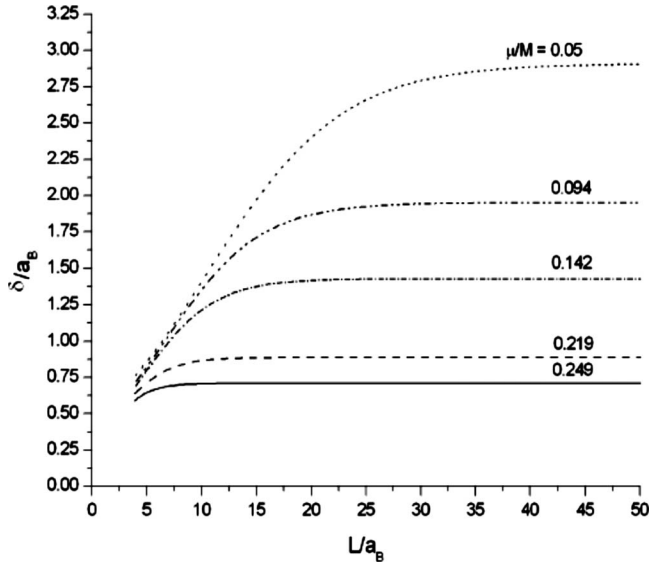

FIG. 3. Transition layer values (δ/a_B) as a function of quantum well thickness (L/a_B) computed for five different masses ratios (μ/M:0.050;0.094;0.142;0.219;0.249).

drogenic limit converges to the correct bulk value for well thicknesses larger than $30a_B$, and shows a small increment (less than 1/100) with respect to its bulk value at $L \approx 7.5a_B$. Notice that also the transition layer value reaches its saturation for $L \approx 10a_B$ in the positronium while well thicknesses as large as $30a_B$ are necessary in order to obtain the hydrogenic limit (Fig. 3).

The asymptotic values of the transition layer for very large quantum wells ($L \to \infty$), as a function of mass ratio, are shown in Fig. 4. We observe that the transition layer is as large as four times the Bohr radius in the limit of hydrogenic masses ratio ($m_h \approx 1836 m_e \Rightarrow \delta \approx 4a_B$) while it is a bit greater than half the Bohr radius in the positronium limit ($M = 4\mu \Rightarrow \delta \approx 0.7a_B$); its behavior is also in agreement with the exact adiabatic exciton envelope function[27] as shown in a previous computation for quantum well in the range of thicknesses $10a_B \leq L \leq 20a_B$ (see Fig. 3, Ref. 30 where the two

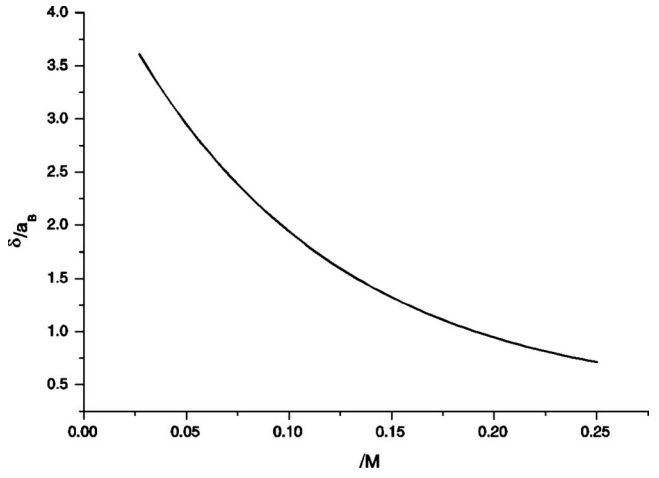

FIG. 4. Saturation value of the transition layer ($\delta_{L\to\infty}/a_B$) as a function of mass ratio μ/M.

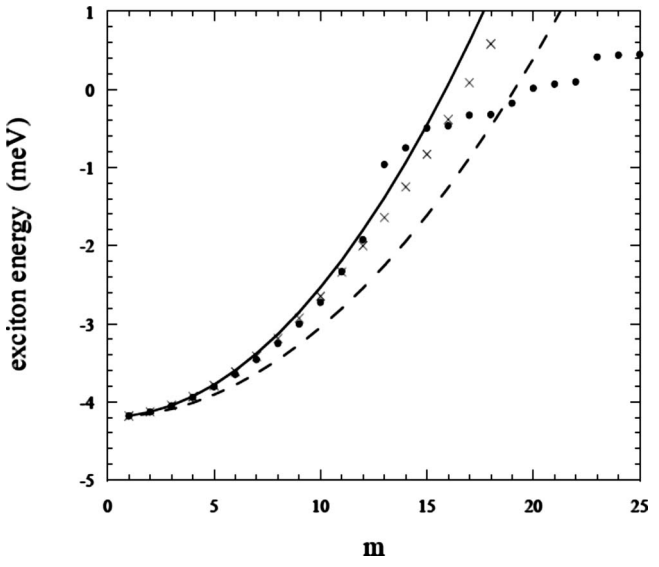

FIG. 5. Heavy-hole exciton energy as a function of center-of-mass quantum number m in a AlGaAs/GaAs(001) quantum well of thickness $L=250$ nm. The energy is computed by full theory (dots), analytical model (crosses), and hard-sphere model with (solid curve) and without dead layer (dashed curve).

curves must be exchanged). We would like to remind that a former evaluation,[27] derived from the energy balance equation: $-R^*(a) + \frac{\hbar^2}{2M}K_m^2 = -\frac{\hbar^2}{2M}(\frac{1}{\delta})^2$, at the continuum limit of the hydrogenic set of states gives not a correct behavior of the transition layer[28] as a function of exciton masses ratio (see also Ref. 30 and the discussion therein).

Notice that exciton transition layer of Fig. 4, computed in the limit of slab thickness $L \to \infty$, should be equal to those in semi-infinite sample of Eq. (1). Therefore, the former choice can reconcile the transition layer effect in semi-infinite samples[34,35] and in slabs,[25] without introducing a further "*ad hoc*" dead layer (added to the transition layer) as hypothesized in Ref. 34.

We have observed before that in the analytical model of Eqs. (5a) and (5b) the most intriguing approximation is the hydrogenic series truncation adopted. In the present paper, the correct energy location of the average virtual state[27] is obtained by comparing the analytical model with the full theory of Ref. 31.

In Figs. 5 and 6 the heavy- and light-hole exciton energies, computed by the full theory of Ref. 31 and by the former analytical model for a quantum well of thickness $L=20a_B=250$ nm are given as a function of an energy order parameter m that in the case of our analytical model coincides with the center-of-mass quantum number. The physical parameters adopted in the calculations are the same of Ref. 36, and the minimized parameters are $a_{lh} = 19.977 \pm 0.002$ nm and $a_{hh} = 12.483 \pm 0.002$ nm for light- and heavy-hole effective Bohr radii respectively, and $\delta_{lh} = 14.277 \pm 0.002$ nm and $\delta_{hh} = 21.133 \pm 0.002$ nm for the corresponding transition layers.

We observe, from Figs. 5 and 6, that the contribution of $n=2$ hydrogenic function becomes important for heavy-hole exciton states with the center-of-mass quantum number greater than $m > 12$ corresponding to the exciton energy

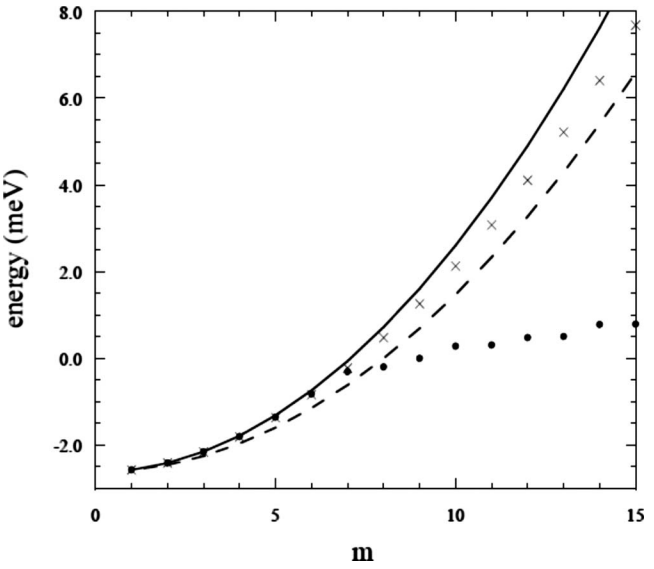

FIG. 6. Light-hole exciton energy as a function of center-of-mass quantum number m in a AlGaAs/GaAs(001) quantum well of thickness $L=250$ nm. The energy is computed by full theory (dots), analytical model (crosses), and hard-sphere model with (solid curve) and without dead layer (dashed curve).

~ 2.3 meV greater than the heavy-hole $m=1$ state, and analogously for light-hole states $m>8(\sim 3.8$ meV). Therefore, the analytical model, also in its lowest order of formulation,[25] should be able to reproduce the optical response in this range of quantum well dimensions since both the former ranges of energy are greater than those shown in the experimental spectra [see Fig. 14(b)] of Schneider *et al.*[33]

Finally, in Figs. 5 and 6 also the hard-sphere model energies, computed with and without $(d\rightarrow 0)$ the dead-layer effect, are shown. The rather sound agreement between the full theory and the hard-sphere model with dead-layer effect for the lower m values is essentially due to the values adopted in the present calculation that coincide with the transition layer values obtained by a variational minimization (namely, $\delta_{hh}=1/\bar{P}_{hh}\approx 21.1$ nm and $\delta_{lh}=1/\bar{P}_{lh}\approx 14.4$ nm) while those computed with the hard-sphere interpolation equation: $d=(1-2\mu/M)a_B$ are strongly different from the former ones ($d_{hh}\approx 10$ nm and $d_{lh}\approx 6.5$ nm for heavy- and light-hole excitons, respectively).

Now, let us compute the lowest energy envelope function of an exciton in the hydrogenic limit $(m_h\rightarrow\infty)$ for the heavy hole trapped at the site $Z_o=0$ of a rather large quantum well $(L=20a_B)$. The analytical envelope function is: $\Psi_m(z;Z_o=0)=N_m g_m(z;Z_o=0)\varphi_{1S}(r)$ and, for transition layer limit $\delta\rightarrow 0(\bar{P}\rightarrow\infty)$, the exciton energy converges to the bulk value. Indeed, in this limit, from Eqs. (5a) and (5b), we obtain $tg(K_m L/2)\rightarrow -\infty$ and $tg(K_m L/2)=0$, respectively, therefore the wave-vector quantization of the electron is $K_m=\frac{\pi}{L}m$ for $m=1,2,3,\ldots$ In Appendix B the first momentum of the lowest energy state of the trapped exciton Hamiltonian in a large quantum well is given in an analytical form. The bulk exciton energy can be obtained also by a variational minimization as a function of effective Bohr radius $a=a_B=10.8711\pm 0.002$ nm and the effective Rydberg is Ryd$=-4.81173$ meV. In Fig. 7, the confinement function $g_1(z;Z_o=0)$ is computed as a function of the electron-hole relative motion along z axis. Notice that, at variance of a simple cosine function that describes electron confinement in a 2D quantum well,[26] this function shows a rather flat shape, except at the interfaces $(Z\approx\pm L/2)$ and, as fully discussed in Refs. 26 and 27, this behavior is a fingerprint that the present analytical model is well suited for describing the center-of-mass quantization. In Fig. 8 we compute the former system by imposing a transition layer value different from zero ($\delta=21.133$ nm); also in this case the shape remains rather smooth but the transition layer effect is clearly shown at the boundaries of the well.

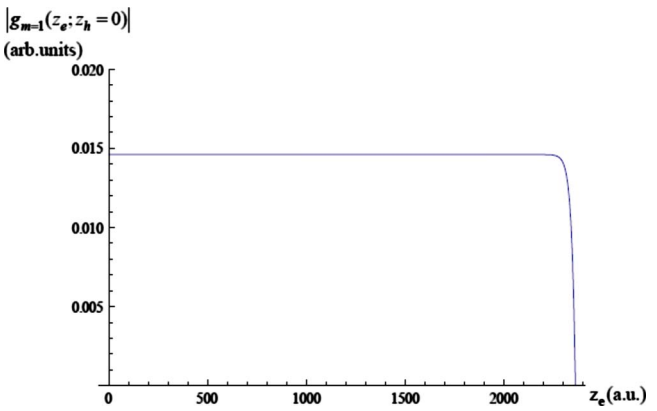

FIG. 7. (Color online) Trapped exciton confinement function $|g_{m=1}(z_e;z_h=0)|$ [Eq. (B2))] of AlGaAs/GaAs(001) quantum well of thickness $L=250$ nm as a function of electron Z coordinate with transition layer $\delta\rightarrow 0$.

In conclusion we would like to remind that the optical response of exciton polaritons is strongly dependent, not only on the exciton energy but also on its envelope function shape. Therefore for very large quantum wells $(L\geq 20a_B)$ the former analytical model should be able to describe the optical experimental measurements of Ref. 33.

In order to generalize the former model, also in the zone very close to the quantum well thicknesses $5a_B\leq L\leq 10a_B$, we will have to extend the finite sum of Eq. (3) to higher

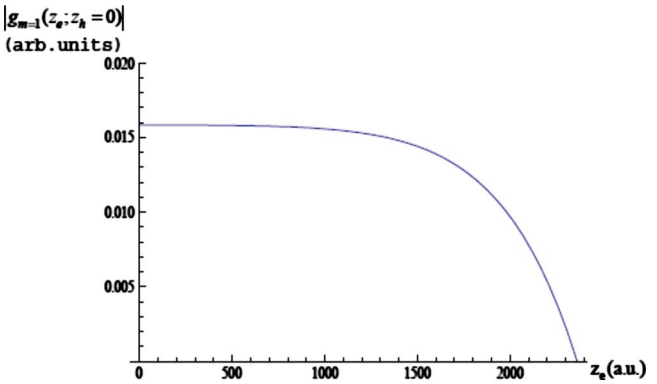

FIG. 8. (Color online) Trapped exciton confinement function $|g_{m=1}(z_e;z_h=0)|$ of AlGaAs/GaAs(001) quantum well of thickness $L=250$ nm as a function of electron Z coordinate with transition layer $\delta=21.16$ nm.

energies of the hydrogenic wave function, as discussed in Appendix A. Moreover, since the real symmetric matrix Hamiltonian is rather diagonal only for large wells, in this range of thicknesses, we must solve a generalized eigenvalue problem, namely, $\overleftrightarrow{A}\vec{\Psi}=E\overleftrightarrow{B}\vec{\Psi}$, where $\langle\Psi_n|\hat{H}_{ex}|\Psi_m\rangle=\langle\Psi_m|\hat{H}_{ex}|\Psi_n\rangle=\overleftrightarrow{A}$ and the matrix of the normalized exciton states is quasiunit real symmetric matrix $\langle\Psi_n||\Psi_m\rangle=\langle\Psi_m||\Psi_n\rangle=\overleftrightarrow{B}$. Notice that the generalized analytical envelope function is not a pure state of the center-of-mass wave vector, even if it still remains under the one-transition layer approximation. In conclusion, we have pointed out that the analytical model is essentially based on a smart truncation of the hydrogenic basis set expansion, and it must be implemented (see Appendix A) to correctly take into account the Wannier exciton dynamics in all the range of thickness till the semi-infinite limit ($5a_B \leq L \leq \infty$).

III. OPTICAL RESPONSE OF A SINGLE QUANTUM WELL UNDER THE CENTER-OF-MASS QUANTIZATION

In this section, the exciton-polariton propagation in a single quantum well under center-of-mass quantization is computed by the former analytical exciton model in a large range of quantum well thicknesses ($5a_B \leq L \leq 20a_B$), and compared with the full theories of Refs. 31, 33, and 36, and with the heuristic hard-sphere model. Moreover, we will compute self-consistently the polariton propagation in a slab in order to reproduce, without introducing fitting parameters (except the homogeneous nonradiative broadening), the experimental transmission spectra in the high-quality GaAs samples of Schneider *et al.*[33]

First of all, let us consider a GaAs quantum well of thickness $L=5a_B=62.5$ nm, that is in the non-adiabatic zone, as discussed in the former section. The parameter values, adopted for the calculation, are taken from Ref. 36, namely, $m_e=0.067m_o$, $m_{hh}=0.457m_o$, background refraction index $n_b=3.71$, energy gap $E_{gap}=1.42$ eV, and nonradiative broadening $\Gamma=0.03$ meV. The electric dipole moment is replaced by the Kane's energy[39] ($E_K=22.71$ eV for GaAs) that is conceptually more suitable than the electric dipole moment for describing the radiation-matter interaction in translational periodic systems.

The transmittance spectrum is computed by a self-consistent solution of Schroedinger-Maxwell equations in the effective-mass approximation, as reported in Ref. 30, where all the analytical formula necessary for the calculation are given explicitly. The Fabry-Perot effect is suppressed in the spectra[33,36] by using the same background dielectric function in whole the space; this allows to observe exciton-polariton peaks free from the interferences due to the Fabry-Perot oscillations.[33] In Fig. 9 the absorption spectrum is shown for the lowest five polariton states; the energy positions of the optical peaks are labeled with the same quantum number m of the corresponding center-of-mass exciton state ($m=1-5$). For this quantum well thickness ($L=\lambda/4$) the even and odd exciton-polariton states show almost comparable intensities.

The phase of the transmittance amplitude is shown in Fig. 10. Notice that the maxima of the absorption are in correspondence of the inflection points of the phase curve; therefore, there is a complete correspondence in the polariton spectra between phase and intensity. To properly reproduce both these quantities is a very severe check for the exciton model adopted in the calculation as fully discussed in Ref. 33 and underlined in the present theory versus the experimental results.

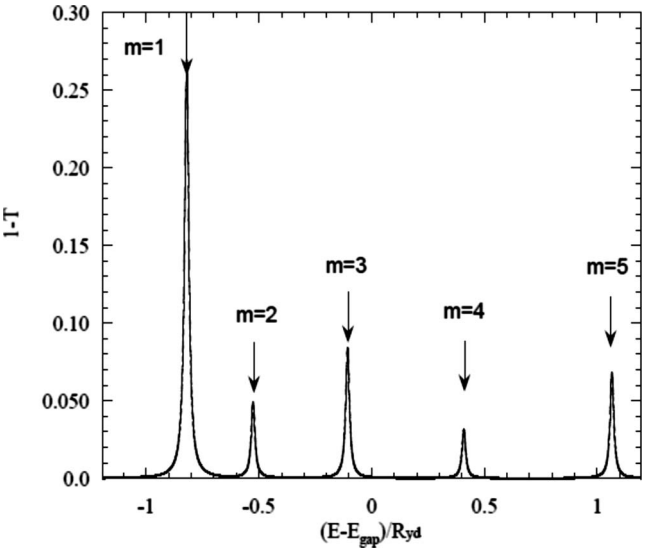

FIG. 9. Optical absorbance $(1-T)$ of the heavy-hole exciton as a function of photon energy $[(E-E_{gap})/\mathrm{Ryd}]$ in AlGaAs/GaAs(001) quantum well of thickness $L=62.5$ nm.

Now, let us compare the exciton energies computed by the analytical model with those derived by the full theory of Ref. 31. In Fig. 11 these exciton energies are shown as a function of the quantum number m of the center-of-mass motion. The minimized effective Bohr radius and transition layer of the analytical model are $a=12.464\pm0.002$ nm and $\delta=1/\bar{P}$

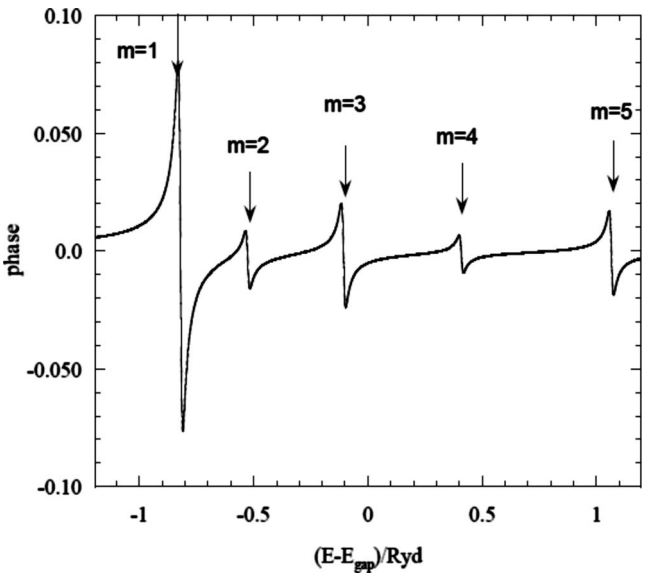

FIG. 10. Phase of the optical absorbance of the heavy-hole exciton as a function of photon energy $[(E-E_{gap})/\mathrm{Ryd}]$ in AlGaAs/GaAs(001) quantum well of thickness $L=62.5$ nm.

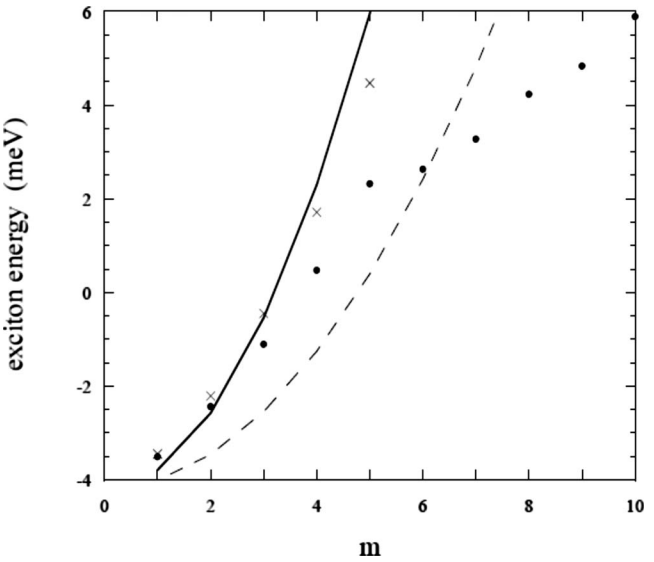

FIG. 11. Heavy-hole exciton energy as a function of center-of-mass quantum number m in AlGaAs/GaAs(001) quantum well of thickness $L=62.5$ nm. The energy is computed by full theory (dots), analytical model (crosses), and hard-sphere model with (solid curve) and without dead layer (dashed curve).

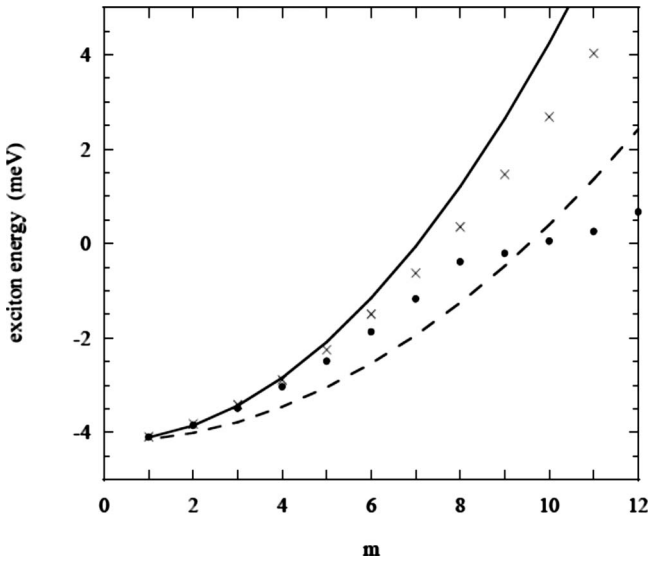

FIG. 12. Heavy-hole exciton energy as a function of center-of-mass quantum number m in AlGaAs/GaAs(001) quantum well of thickness $L=125$ nm. The energy is computed by full theory (dots), analytical model (crosses), and hard-sphere model with (solid curve) and without dead layer (dashed curve).

$=10.228\pm0.002$ nm, respectively. The exciton energy computed with the simple hard-sphere model are also reported for vanishing dead layer and for a dead layer as large as the minimized transition layer value. We note a rather large energy difference (about 1.23 meV for $m=4$) between analytical model and full theory in correspondence with higher energy states ($m\geq4$) that rapidly decreases for the lower energy states; for instance for $m=3$ it drops to 0.6 meV and for $m=2$ is about 0.2 meV. The last value is rather acceptable if we take into account that the nonradiative broadening is about $\Gamma_{NR}=0.5-1.0$ meV in typical samples and $\Gamma_{NR}\approx0.25$ meV in high quality quantum wells. Obviously, the large discrepancy observed for the high-energy states is not surprising if we take into account that the exciton envelope functions of the analytical model, labeled with the quantum number m, are pure states of the center of mass while the exciton states of the full theory are a general superposition of states with different center-of-mass wave vectors and are expanded on a rather complete set of the relative motion wave functions.

In conclusion, in this thicknesses range of values the lowest exciton states are in sound agreement with those obtained by the full theory while for describing higher energy states of the center of mass ($m\geq4$) we will have to implement the simple analytical model as discussed at the end of the former section. Moreover, we observe that the full theory gives exciton states located between the two curves of the hard-sphere model with and without the dead-layer effect and this leads to the well-known possibility of recovering the rather correct exciton energies by using the Pekar's dead layer as a fitting parameter. Now, let us consider GaAs quantum wells in the zone of the center-of-mass quantization $10a_B\leq L\leq20a_B$. In Fig. 12 the exciton energies of the analytical model and of the full theory[31] in a single quantum well of thickness $L=10a_B=125$ nm are shown as a function of the center-of-mass quantum number m. The physical parameters values are the same of the former sample, and the minimized variational parameters are $a=12.560\pm0.002$ nm and $\delta=1/P=16.400\pm0.002$ nm. We observe that, while the effective Bohr radius is very close to the 3D Bohr radius, the transition layer value is rather different from its saturation value, underlining the strong influence of the transition layer effect on the exciton dynamics in this range of thicknesses. The calculation confirms a negligible difference between the two models for the lower energy states ($m\leq4$) and an increase in this difference till 0.75 meV for the $m=8$ state where higher energy ($n>1$) hydrogenic states cannot be neglected. In fact, exciton states with $m\geq8$ drop into the second parabolic curve due to the $n=2$ hydrogenic states, therefore the agreement between the analytical model and the full theory can be improved along the line discussed in Appendix A. In Fig. 12 also the exciton energies computed by Pekar's model with and without dead layer are shown for sake of comparison.

In Fig. 13 the optical spectra, computed self-consistently with the analytical exciton envelope function and with the full exciton model, are shown; due to the photon wavelength that is about $\lambda\approx2L$ the odd exciton functions ($m=2,4,6,\ldots$) give a stronger contribution than the even ($m=1,3,7,\ldots$) ones. In fact, in the computed spectrum of the full exciton theory[31] the intensity of $m=7$ exciton-polariton peak is vanishingly small while it is shifted toward the higher energies for the analytical model. We would like to underline that the transmission spectrum computed by our full theory is in very good agreement, both in energy positions and in line shapes, also with those computed by the full theories of Refs. 33 and 36, not reported here.

In order to go a bit deeper in the optical spectrum analysis, notice that the double peak, due to the lowest exciton energies ($m=1,2$), is very sensitive to the radiation-matter

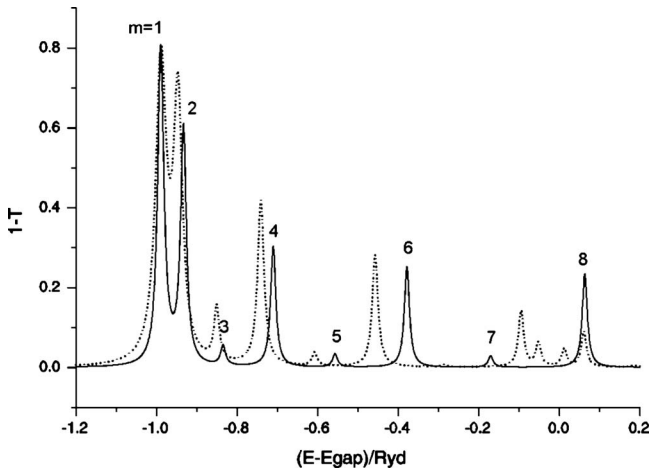

FIG. 13. Optical absorbance $(1-T)$ of the heavy-hole exciton as a function of photon energy $[(E-E_{gap})/\mathrm{Ryd}]$ in AlGaAs/GaAs(001) quantum well of thickness $L=125$ nm: full theory (dashed curve) and analytical model (solid curve).

interaction. Moreover, due to the small nonradiative broadening value adopted in the calculation, we can appreciate the difference in energy between the analytical model and the full theory for all the range of energies of the polariton spectrum even if theirs values remain in any case rather small for $m<8$ exciton-polariton states. In fact, let us consider the two peaks for $m=6$: they seem very well separated in the spectrum but the energy difference (<0.4 meV) is lower than the optical broadening (see also Fig. 12).

Finally, we would like to underline that in the range of energies reported in Fig. 13 our microscopic model gives a more accurate result than that based on Pekar's ABC. In fact, in Ref. 36 (see Fig. 4) the energy difference between full theory and Pekar's model for $m=6$ exciton-polariton state is about 0.7 meV, that is two times our difference, and it is greater than the broadening value. Therefore, we can conclude that our analytical model can reproduce the full theory till $m\leq 6$ exciton-polariton state and that, in any case, it gives a better agreement with the full theories than that obtained by Pekar's model.[36]

Now, let us try to reproduce the experimental transmission spectrum of a high-quality GaAs quantum well reported in the work of Schneider *et al.*[33] by our analytical self-consistent theory. In Fig. 7b of Ref. 33, reproduced here in Fig. 14(b), many peaks due to the center-of-mass quantization of both heavy- and light-hole excitons in a large quantum well of GaAs ($L=20a_B=250$ nm) are clearly shown by arrows. We would like to underline that we have chosen to reproduce the experimental results of Schneider *et al.*[33] because they are well suited for checking the present analytical model. In fact, the Wannier exciton is perfectly confined in a self-sustained quantum well, and the Fabry-Perot effect, due to the modulation of the background dielectric function, is suppressed by the presence of antireflection coating on both the sample surfaces. Moreover, in a large quantum well the anisotropic electron-hole masses induce a very small energy shift on the exciton energies, therefore, we can use isotropic exciton masses in the present range of thicknesses.

In the former section, we have shown that the analytical exciton model is in perfect agreement with the full theory[31]

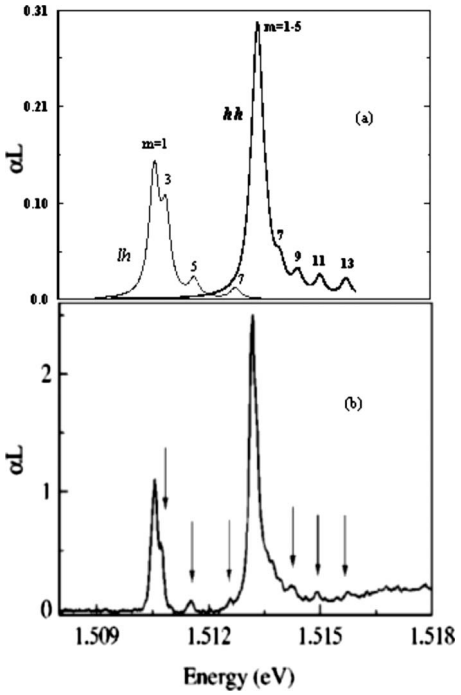

FIG. 14. (a) Optical absorbance $(1-T)$ computed for light- and heavy-hole excitons as a function of photon energy in AlGaAs/GaAs(001) quantum well of thickness $L=250$ nm. (b) Experimental optical absorbance of light- and heavy-hole excitons of Ref. 33 as a function of photon energy in AlGaAs/GaAs(001) quantum well of thickness $L=250$ nm.

in a sufficient large range of energies (9 meV), and this is well suited for reproducing the experimental spectrum of Ref. 33. The parameter values adopted for the calculation are[33] $L=20a_B=250$ nm, $m_e=0.067$, $m_{hh}=0.457m_o$, $m_{lh}=0.080m_o$, $E_{gap}^{lh}=1.5105$ eV, $n_b=3.71$, $E_{gap}^{hh}=1.5130$ eV, and Kane's energy $E_K=22.71$ eV; the minimized parameter values, given in the former section (see also Figs. 5 and 6), underline the different behaviors, from positronium for light hole to hydrogenic atom for heavy hole, of Wannier excitons. The energy shift between heavy- and light-hole energy gaps, due to the residual strain of the sample, is discussed and evaluated in Ref. 33.

The high quality ($\Gamma_{NR}\leq 0.25$ meV) of the samples should allow to study the effect induced by the wave-vector quantization of the center-of-mass motion at $T=2$ K. Indeed, the polariton effect is important only in the case where the exciton broadening value is less than a critical value,[14] namely, $\Gamma_c=[\frac{8\Delta_{LT}E_{ex}^2\varepsilon_b}{Mc^2}]^{1/2}$, that for the parameters chosen is $\Gamma_c\approx 0.21$ meV. Notice that the nonradiative broadening value chosen in the present calculation, in order to reproduce the experimental spectra line shapes ($\Gamma_{NR}=0.15$ meV), is in rather close agreement with that given in Ref. 33 and, moreover, since $\Gamma<\Gamma_c$, exciton-photon coupling becomes dominant with respect to the exciton acoustic phonon interaction. Since the exciton is computed in a simple two-band model, the optical response of heavy- and light-hole exciton polaritons will be shown in the pictures by different curves but in the same energy scale.

The absorption of light- and heavy-hole excitons are shown in Fig. 14(a). We would like to underline that the

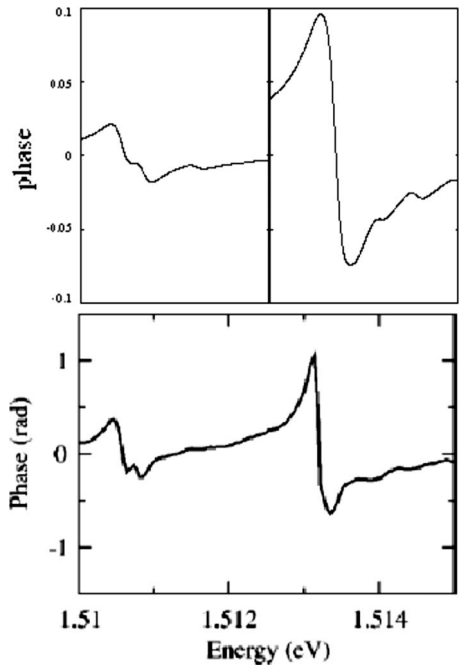

FIG. 15. (a) Phase of the optical absorption computed for light- and heavy-hole excitons as a function of photon energy in AlGaAs/GaAs(001) quantum well of thickness $L=250$ nm. (b) Measured phase of the optical absorption (Ref. 33) of light- and heavy-hole excitons as a function of photon energy in AlGaAs/GaAs(001) quantum well of thickness $L=250$ nm.

agreement between theory and experiment is very good both in the line shapes and in energy positions, as shown by the arrows in correspondence of the maxima of the experimental spectrum of Schneider[33] reported in Fig. 14(b). In fact, the characteristic double peak of the light-hole exciton polariton and the asymmetric line shape of the main peak of the heavy hole, due to the interplay of polaritonic effect and center-of-mass quantization of the Wannier exciton, are clearly reproduced. This agreement is particularly meaningful when we take into account that it is obtained for the same parameter values in the presence of rather different exciton dynamics. In fact, light-hole exciton is close to positronium limit ($\mu/M=0.248$) while the heavy hole is rather close to the hydrogenic behavior ($\mu/M=0.111$). Moreover, the analytical model allows to unambiguously assign the center-of-mass character for any features present in the experimental spectrum. For instance, the peak at $m=7$, not assigned in Ref. 33, has even-parity character, due to the photon wavelength ($L\approx\lambda$) that gives odd exciton-polariton peaks negligible small in the spectrum. Finally, notice that for the heavy-hole exciton polariton in Ref. 33 [see Fig. 10(c)] the $m=11$ peak is shifted toward the lower energy side, with respect to the experimental spectrum while the $m=13$ one is out of the energy scale.

In Figs. 15(a) and 15(b) the computed phase of exciton-polaritons absorption spectrum and the corresponding experimental results of Ref. 33 are shown, respectively. Also in this case the agreement between theory and experiment is sound both for energy positions and line shapes. Obviously, the long tail shown by the heavy-hole exciton-polariton phase toward the lower photon energies cannot be matched with the light-hole phase by the simple two-band model. Moreover, all the features observed in the absorption spectrum have a counterpart in the phase spectrum and also the characteristic two peaks feature of the light-hole exciton polariton and the center-of-mass peaks at higher energies are reproduced. In conclusion, the simultaneous measurements of phase and transmission spectra allow to assign the exciton-polariton peaks of the experimental spectrum to the pure center-of-mass exciton-polariton quantization.

We would like to underline that in Ref. 33 the authors compare the optical properties, computed by their accurate microscopic exciton model, with a number of heuristic models, based on different ABCs, in order to conclude that "A simultaneous description of the measured amplitude and phase of the transmitted electric field is only possible with a *full* model." The sound agreement between our analytical microscopic model, based on the one-transition layer approximation, and the experimental results of Ref. 33 strongly suggest the replacement of the adjective full with *microscopic*.

IV. CONCLUSIONS

In the present work the analytical microscopic exciton model in a large ($L\gg a_B$) single quantum well, proposed in Ref. 25 is revised and implemented in order to reproduce the Wannier exciton center-of-mass quantization in the range of quantum well thicknesses $5a_B\leq L\leq\infty$.

The microscopic transition layer effect, observed at the well/barrier interfaces in a single quantum well, is discussed at variance of the classical dead layer introduced by Pekar[21] and compared with various full theoretical models.[31,33,36] Moreover, this new formulation has allowed to reconcile the Wannier exciton dynamics in large quantum wells ($L\gg a_B$) and in semi-infinite semiconductor samples ($L\rightarrow\infty$) described by the same analytical microscopic model.[25,34]

Finally, exciton-polariton transmission spectra in large quantum wells ($L=20a_B$) are computed and compared with experimental results in high-quality GaAs samples obtained by Schneider *et al.*[33] The sound agreement between theory and experiment has allowed to unambiguously assign the transmission spectra peaks to the pure states of the exciton center-of-mass quantization.

ACKNOWLEDGMENT

The authors are indebted to E. Vuzza for technical support during the manuscript preparation.

APPENDIX A: A GENERALIZED VARIATIONAL WANNIER EXCITON ENVELOPE FUNCTION

We generalize the Wannier exciton envelope function expanding Eq. (2) of the text by taking into account also the $2s$ hydrogenic function. Since $2s$ is symmetric with respect to the z axis we can adopt the same procedure of Sec. II based on the following three steps.

(1) From the relationship $\hat{\mathbb{R}}\Psi_E(\vec{r},Z)=\pm\Psi_E(\vec{r},Z)$ we obtain the even and odd envelope functions, namely,

$$\Psi_E^e(\vec{r},Z)=\alpha_1\Phi_E^e(\vec{r},Z)+2\sum_{nlm}^{n>2}[\alpha_{nlm}\cosh(P_nZ)\varphi_{nlm}^e(\vec{r}) - \beta_{nlm}\sinh(P_nZ)\varphi_{nlm}^o(\vec{r})], \tag{A1a}$$

$$\Psi_E^o(\vec{r},Z)=\beta_1\Phi_E^o(\vec{r},Z)+2\sum_{nlm}^{n>2}[\alpha_{nlm}\cosh(P_nZ)\varphi_{nlm}^o(\vec{r}) - \beta_{nlm}\sinh(P_nZ)\varphi_{nlm}^e(\vec{r})], \tag{A1b}$$

where $\alpha_1=\alpha_{100}$ and $\beta_1=\beta_{100}$; the functions $\Phi_E^i(\vec{r},Z)$ for $i=e,o$ are

$$\Phi_E^e(\vec{r},Z)=\cos(K_1Z)\varphi_{1s}(r)+\tilde{\alpha}_{200}\cos(K_2Z)\varphi_{2s}(r), \tag{A2a}$$

$$\Phi_E^o(\vec{r},Z)=\sin(K_1Z)\varphi_{1s}(r)+\tilde{\beta}_{200}\sin(K_2Z)\varphi_{2s}(r), \tag{A2b}$$

where $\tilde{\alpha}_{200}=\alpha_{200}/\alpha_1$ and $\tilde{\beta}_{200}=\beta_{200}/\beta_1$. Indeed, the functions of Eqs. (A1a) and (A1b) will be reduced to Eqs. (A4a) and (A4b), respectively, for $\alpha_{200}=\beta_{200}=0$.

By adopting the one-transition layer approximation an average value for the inverse of the transition layer depth, $P_{n>2}=P=1/\delta$ is taken and the envelope functions assume the following analytical form:

$$\Psi_E^e(\vec{r},Z)=N_e[\Phi_E^e(\vec{r},Z)+\cosh(PZ)F_{ee}(\vec{r})-\sinh(PZ)F_{eo}(\vec{r})], \tag{A3a}$$

$$\Psi_E^o(\vec{r},Z)=N_o[\Phi_E^o(\vec{r},Z)+\cosh(PZ)F_{oo}(\vec{r})-\sinh(PZ)F_{oe}(\vec{r})], \tag{A3b}$$

where $N_e=\alpha_1$ and $N_o=\beta_1$.

(2) We impose the NEBCs: $\Psi_E(z_e=\pm L/2,z_h,\vec{\rho})=\Psi_E(z_h=\pm L/2,z_e,\vec{\rho})=0.0$ in order to compute the F functions. For the even solution $\Psi_E^e(\vec{r},Z)$, Eq. (A3a), we obtain

$$F_{ee}(\vec{r})=f_{ee}(K_1)\varphi_{1s}(\vec{r})+\tilde{\alpha}_2f_{ee}(K_2)\varphi_{2s}(\vec{r}), \tag{A4a}$$

$$F_{eo}(\vec{r})=f_{eo}(K_1)\varphi_{1s}(\vec{r})+\tilde{\alpha}_2f_{eo}(K_2)\varphi_{2s}(\vec{r}) \tag{A4b}$$

for $0\le z\le L/2$, $Z_1(z)=\alpha_e z-L/2$, and $Z_2(z)=-\alpha_h z+L/2$. The f functions for even exciton functions are

$$f_{ee}(K)=\frac{\cos(KZ_2)\sinh(PZ_1)-\cos(KZ_1)\sinh(PZ_2)}{\sinh[P(Z_2-Z_1)]}, \tag{A5a}$$

$$f_{oe}(K)=\frac{\sin(KZ_2)\cosh(PZ_1)-\sin(KZ_1)\cosh(PZ_2)}{\sinh[P(Z_2-Z_1)]} \tag{A5b}$$

and analogously for the odd ones,

$$f_{oo}(K)=\frac{\sin(KZ_2)\sinh(PZ_1)-\sin(KZ_1)\sinh(PZ_2)}{\sinh[P(Z_2-Z_1)]}, \tag{A6a}$$

$$f_{eo}(K)=\frac{\cos(KZ_2)\cosh(PZ_1)-\cos(KZ_1)\cosh(PZ_2)}{\sinh[P(Z_2-Z_1)]}. \tag{A6b}$$

(3) From the continuity of the exciton wave function and its first derivative at the $z=0$ surface we obtain the conditions for the center-of-mass quantization. Also in this case, due to the symmetry properties of the different components of the envelope functions, the center-of-mass quantization must accomplish the two following relationships: $\frac{\partial f_{ee}}{\partial z}\big|_{z=0}=0$ and $\frac{\partial f_{eo}}{\partial z}\big|_{z=0}=0$ for the even exciton function (analogously for the odd one). It is simple to check that the center-of-mass wave vector K follows the even dispersion: $K_m^e tg[K_m^eL/2]+Ptgh[PL/2]=0$ for $m=1,3,5,\ldots$ and the odd one, $Ptg[K_m^oL/2]-K_m^otgh[PL/2]=0$ for $m=2,4,6,\ldots$, according to the even $[f_{ee}(z),f_{oe}(z)]$ and odd $[f_{oo}(z),f_{oe}(z)]$ f functions, respectively. The generalized even $(m=1,3,5,\ldots)$ exciton function of Eq. (A3a), assumes the analytical form,

$$\Psi_{m_1,m_2}^e(\vec{r},Z)=N_{m_1,m_2}^e\{\cos(K_{m_1}Z)\varphi_{1s}(\vec{r})+\tilde{\alpha}_2\cos(K_{m_2}Z)\varphi_{2s}(\vec{r}) + \cosh(PZ)[f_{ee}(K_{m_1})\varphi_{1S}(r) + \tilde{\alpha}_2f_{ee}(K_{m_2})\varphi_{2S}(r)]+-\sinh(PZ) \times[f_{eo}(K_{m_1})\varphi_{1S}(r)+\tilde{\alpha}_2f_{eo}(K_{m_2})\varphi_{2S}(r)]\} \tag{A7}$$

and analogously for the odd Wannier exciton function.

Notice that the inclusion in the analytical model of the $2s$ hydrogenic function not only increases the number of variational parameters but also gives off-diagonal envelope function components in the center-of-mass wave vector.

The inclusion in the model of $2p$ hydrogenic functions is a bit more tricky since the finite sum is composed of two even components $(2p_x,2p_y)$ but also of an odd one $(2p_z)$. Therefore, the generalized envelope functions should mix even and odd center-of-mass wave vectors. In fact, let us choose (ℓ,f,ζ) as the direction cosines of the relative motion coordinate with respect to the Cartesian axis: $\varphi_{2p}(\vec{r})=\ell\varphi_{2p_x}(\vec{r})+f\varphi_{2p_y}(\vec{r})+\zeta\varphi_{2p_z}(\vec{r})$. In this case Eqs. (A2a) and (A2b) become

$$\Phi_E^e(\vec{r},Z)=\cos(K_{100}Z)\varphi_{1s}(r)+\tilde{\alpha}_{200}\cos(K_{200}Z)\varphi_{2s}(r) + \tilde{\alpha}_{211}\cos(K_{211}Z)[\ell\varphi_{2p_x}(\vec{r})+f\varphi_{2p_y}(\vec{r})] + \zeta\tilde{\beta}_{210}\sin(K_{210}Z)\varphi_{2p_z}(\vec{r}), \tag{A8a}$$

$$\Phi_E^o(\vec{r},Z)=\sin(K_{100}Z)\varphi_{1s}(r)+\tilde{\beta}_{200}\sin(K_{200}Z)\varphi_{2s}(r) + \tilde{\beta}_{211}\sin(K_{211}Z)[\ell\varphi_{2p_x}(\vec{r})+f\varphi_{2p_y}(\vec{r})] + \zeta\tilde{\alpha}_{210}\cos(K_{210}Z)\varphi_{2p_z}(\vec{r}), \tag{A8b}$$

where $\tilde{\alpha}_{200}=\alpha_{200}/\alpha_1$, $\tilde{\alpha}_{211}=\alpha_{211}/\alpha_1$, $\tilde{\beta}_{210}=\beta_{210}/\alpha_1$ and $\tilde{\beta}_{200}=\beta_{200}/\beta_1$, $\tilde{\beta}_{211}=\beta_{211}/\beta_1$, $\tilde{\alpha}_{210}=\alpha_{210}/\beta_1$. Now, let us im-

pose the NEBCs: $\Psi_E(z_e=\pm L/2, z_h, \vec{\rho})=\Psi_E(z_h=\pm L/2, z_e, \vec{\rho})=0.0$ in order to compute the F functions. For the even solution $\Psi_E^e(\vec{r},Z)$ of Eq. (A3a) we obtain

$$F_{ee}(\vec{r}) = f_{ee}(K_{100})\varphi_{1s}(\vec{r}) + \tilde{\alpha}_2 f_{ee}(K_{200})\varphi_{2s}(\vec{r}) + \tilde{\alpha}_{211} f_{ee}(K_{211}) \times[\hat{\ell}\varphi_{2p_x}(\vec{r}) + \hat{f}\varphi_{2p_y}(\vec{r})] + \hat{\zeta}\tilde{\beta}_{210} f_{oo}(K_{210})\varphi_{2p_z}(\vec{r}), \tag{A9a}$$

$$F_{eo}(\vec{r}) = f_{eo}(K_{100})\varphi_{1s}(\vec{r}) + \tilde{\alpha}_2 f_{eo}(K_{200})\varphi_{2s}(\vec{r}) + \tilde{\beta}_{211} f_{oe}(K_{211}) \times[\hat{\ell}\varphi_{2p_x}(\vec{r}) + \hat{f}\varphi_{2p_y}(\vec{r})] + \hat{\zeta}\tilde{\alpha}_{210} f_{oe}(K_{210})\varphi_{2p_z}(\vec{r}). \tag{A9b}$$

Finally, the generalized even $(m=1,3,5,\ldots)$ exciton function derivation proceed as before. Notice that the former generalization leads to increase the number of variational parameters; in fact, while for $n=1$ we have two nonlinear parameters (a,δ), for $n=2$ we have two nonlinear (a,δ) plus three linear $(\tilde{\alpha}_{200},\tilde{\alpha}_{211},\tilde{\beta}_{211})$ parameters of minimization. Analogously for odd exciton state $(m=2,4,6,\ldots)$ and also in this case the solution embodies odd and even center-of-mass wave vectors.

Finally, by adopting the former procedure, we obtain a set of normalized-independent exciton states, and afterward, it is necessary to solve the generalized problem in order to obtain an orthogonal set of states as discussed in Sec. II.

APPENDIX B: TRAPPED EXCITON IN A QUANTUM WELL

Let us consider a Wannier exciton trapped as a neutral atom at the site $\vec{R}_o=(0,0,Z_o)$, whose electron mass is m_e, and the hole mass is taken in the limit $m_{hh}\to\infty$. In this case the Z component of the center-of-mass coordinate is $Z=z_h=Z_o$ while the coordinate of the relative motion is $z=z_e-z_h=z_e-Z_o$; therefore, the motion of the electron along Z axis is confined in the segment: $-Z_o-L/2\le z\le -Z_o+L/2$. Since the envelope function of the trapped exciton has not defined parity, except for the site $Z_o=0$, a general variational trial function can be obtained as a linear superposition of even and odd exciton envelope functions in order to remove the restricted symmetry properties. Here, we adopt a more intuitive procedure observing that even and odd exciton envelope functions, defined in Sec. II, lost their symmetry property if projected into a nonsymmetric domain as the segment $-Z_o-L/2\le z\le -Z_o+L/2$. In this case, $m=1$ envelope function, projected into the segment $-Z_o-L/2\le z\le -Z_o+L/2$, can be used for a variational determination of the effective Bohr radius that should converges to the 3D Bohr radius for large quantum well $(L\gg a_B)$ while the transition layer assumes the limit $\delta\to 0$. Obviously, many physical properties of exciton analytical model have to be redefined for trapped exciton. In fact, the projected envelope function is

$$\Psi_m(\vec{r};Z_o) = N_m g_m(z;Z_o)\varphi_{1S}(r). \tag{B1}$$

For m odd $(m=1,3,5)$ we have

$$g_m(z;Z_o) = \cos(K_m Z_o) + \cosh(PZ_o) f_{ee}(z) - \sinh(PZ_o) f_{eo}(z) \tag{B2}$$

and for m even $(m=2,4,6,\ldots)$,

$$g_m(z;Z_o) = \sin(K_m Z_o) + \cosh(PZ_o) f_{oo}(z) - \sinh(PZ_o) f_{oe}(z), \tag{B3}$$

where the f functions are obtained by imposing the NEBCs at the surfaces of the well $(Z=\pm L/2)$. For $0\le z\le L/2$ the confinement boundaries are $Z_1=-Z_o-L/2=-L/2$ and $Z_2=-Z_o+L/2=-z+L/2$,

$$\tilde{f}_{ee}(z) = [\cos(KZ_1)\sinh(PZ_2) - \cos(KZ_2)\sinh(PZ_1)],$$

$$\tilde{f}_{eo}(z) = [\cos(KZ_1)\cosh(PZ_2) - \cos(KZ_2)\cosh(PZ_1)] \tag{B4}$$

and for $-L/2\le z\le 0$ the confinement boundaries are $Z_1=L/2$ and $Z_2=-z-L/2$,

$$\tilde{f}_{oe}(z) = [\sin(KZ_1)\cosh(PZ_2) - \sin(KZ_2)\cosh(PZ_1)],$$

$$\tilde{f}_{oo}(z) = [\sin(KZ_1)\sinh(PZ_2) - \sin(KZ_2)\sinh(PZ_1)] \tag{B5}$$

and $f_{ij}(z)=\tilde{f}_{ij}(z)/\sinh[P(Z_2-Z_1)]$ for $i,j=e,o$. Remember that the continuity of the exciton envelope function and its first derivative at the surface $z=0$ are the same of those given in Eqs. (5a) and (5b) but in the trapped exciton appears the electron quantization condition at variance of the former case that describes the center-of-mass motion of Wannier exciton.

Taking into account that we have two different analytical equations for $z\ge 0$ and $z\le 0$, the normalization integration is

$$\langle\Psi_m||\Psi_m\rangle = 2\pi\int_0^\infty \rho d\rho\left\{\int_{z_1}^0 dz + \int_0^{z_2} dz\right\} g_m^2(z;Z_o)\varphi_{1S}^2(\sqrt{\rho^2+z^2}) \tag{B6}$$

and the first momentum of trapped exciton Hamiltonian,

$$\hat{H}_{ex}^t = -\frac{\hbar^2}{2\mu}\vec{\nabla}_{\vec{r}}^2 - \frac{e^2}{\varepsilon_b r}$$

is

$$\langle\Psi_m|\hat{H}_{ex}^t|\Psi_m\rangle = -\frac{\hbar^2}{m_e}\frac{1}{a^2}\langle\Psi_m||\Psi_m\rangle + 2\pi\int_0^\infty \rho d\rho\left\{\int_{z_1}^0 dz + \int_0^{z_2} dz\right\}\left\{\frac{\hbar^2}{m_e}\left[\frac{1}{a}-\frac{1}{a_B}\right]g_m^2(z;Z_o) + -\frac{\hbar^2 g_m(z;Z_o)}{2m_e}\left[\left(|z|+\frac{a}{2}\right)\frac{\partial^2 g_m}{\partial z^2} - 2\frac{z}{a}\frac{\partial g_m}{\partial z}\right]\varphi_{1S}^2(\sqrt{\rho^2+z^2}). \tag{B7}$$

The nth derivative with respect to the relative motion along z

axis of the confinement functions $g_m(z;Z_o)$ are

$$\frac{\partial^\ell g_m}{\partial z^\ell} = -\cos(PZ_o)\frac{\partial^\ell f_{ij}}{\partial z^\ell} + \sin(PZ_o)\frac{\partial^\ell \tilde{f}_{ij}}{\partial z^\ell}. \tag{B8}$$

Taking into account that $dZ_2 = -dz$, the derivative are

$$\frac{\partial f_{ij}}{\partial z} = \left\{ Pf_{ij}\cosh[P(Z_2 - Z_1)] + \frac{\partial \tilde{f}_{ij}}{\partial z} \right\} / \sinh[P(Z_2 - Z_1)] \tag{B9}$$

and

$$\frac{\partial^2 f_{ij}}{\partial z^2} = -P^2 f_{ij}(z) + \left\{ \frac{\partial^2 \tilde{f}_{ij}}{\partial z^2} + 2P\frac{\partial f_{ij}}{\partial z} \times \cosh[P(Z_2 - Z_1)] \right\} / \sinh[P(Z_2 - Z_1)]. \tag{B10}$$

Finally, for very large quantum wells the variational energy of trapped exciton recover the 3D Rydberg value while the confinement function $|g_m(z;Z_o)|$ is an asymmetric function except for the hole coordinate $Z_o = z_h = 0$ and $-L/2 \leq z_e \leq L/2$ as discussed in the text (Figs. 7 and 8).

[1] E. L. Ivchenko, A. I. Nesvizhskii, and S. Jorda, Phys. Solid State **36**, 1156 (1994).

[2] T. Stroucken, A. Knorr, P. Thomas, and S. W. Koch, Phys. Rev. B **53**, 2026 (1996).

[3] M. Hübner, J. Kuhl, T. Stroucken, A. Knorr, S. W. Koch, R. Hey, and K. Ploog, Phys. Rev. Lett. **76**, 4199 (1996).

[4] L. Pilozzi, A. D'Andrea, and K. Cho, Phys. Rev. B **69**, 205311 (2004).

[5] N. Tomassini, D. Schiumarini, L. Pilozzi, and A. D'Andrea, Phys. Rev. B **75**, 085317 (2007).

[6] O. A. Egorov, D. V. Skryabin, A. V. Yulin, and F. Lederer, Phys. Rev. Lett. **102**, 153904 (2009).

[7] A. Amo, D. Sanvitto, F. P. Laussy, D. Ballarini, E. del Valle, M. D. Martin, A. Lematre, J. Bloch, D. N. Krizhanovskii, M. S. Skolnick, C. Tejedor, and L. Via, Nature (London) **457**, 291 (2009).

[8] C. Weisbuch, M. Nishioka, A. Ishikawa, and Y. Arakawa, Phys. Rev. Lett. **69**, 3314 (1992).

[9] M. Hübner, J. P. Prineas, C. Ell, P. Brick, E. S. Lee, G. Khitrova, H. M. Gibbs, and S. W. Koch, Phys. Rev. Lett. **83**, 2841 (1999).

[10] A. C. Schaefer and D. G. Steel, Phys. Rev. Lett. **79**, 4870 (1997).

[11] R. Huang, Y. Yamamoto, R. Andre, J. Bleuse, M. Muller, and H. Ulmer-Tuffigo, Phys. Rev. B **65**, 165314 (2002).

[12] D. Goldberg, L. I. Deych, A. A. Lyyansky, Z. Shi, V. M. Menon, V. Tokranov, M. Yakimov, and S. Oktyabrsky, Nat. Photonics **3**, 662 (2009).

[13] P. Halevi, *Spatial Dispersion in Solids and Plasma* (North-Holland, Amsterdam, 1992), Vol. 1, p. 339.

[14] A. Tredicucci, Y. Chen, F. Bassani, J. Massies, C. Deparis, and G. Neu, Phys. Rev. B **47**, 10348 (1993); G. Czajkowski, F. Bassani, and A. Tredicucci, *ibid.* **54**, 2035 (1996).

[15] H. Tuffigo, R. T. Cox, N. Magnea, Y. Merle d'Aubignè, and A. Million, Phys. Rev. B **37**, 4310 (1988).

[16] N. Tomassini, A. D'Andrea, R. Del Sole, H. Tuffigo-Ulmer, and R. T. Cox, Phys. Rev. B **51**, 5005 (1995).

[17] K. Henneberger, Phys. Rev. Lett. **80**, 2889 (1998).

[18] E. A. Muljarov and R. Zimmermann, Phys. Rev. B **66**, 235319 (2002).

[19] S. Schumacher, G. Czycholl, F. Jahnke, I. Kudyk, H. I. Ruckmann, J. Gutowski, A. Gust, G. Alexe, and D. Hommel, Phys. Rev. B **70**, 235340 (2004).

[20] V. A. Fonoberov and A. A. Balandin, Phys. Rev. B **70**, 195410 (2004).

[21] S. I. Pekar, Sov. Phys. JETP **6**, 785 (1958).

[22] J. J. Hopfield and D. G. Thomas, Phys. Rev. **132**, 563 (1963).

[23] A. D'Andrea and R. Del Sole, Phys. Rev. B **25**, 3714 (1982).

[24] A. D'Andrea and R. Del Sole, Phys. Rev. B **29**, 4782 (1984); **32**, 2337 (1985); **38**, 1197 (1988).

[25] A. D'Andrea and R. Del Sole, Phys. Rev. B **41**, 1413 (1990).

[26] M. Combescot, R. Combescot, and B. Roulet, Eur. Phys. J. B **23**, 139 (2001).

[27] M. Combescot, R. Combescot, and B. Roulet, Eur. Phys. J. B **22**, 89 (2001).

[28] Notice that the choice of $n \to \infty$ for $N-1$ degenerate virtual states, not strictly necessary for the consistency of the theory, gives two unpleasant results, namely, (i) a too small transition layer value in the hydrogenic limit ($\mu/M \to 0$), as underlined in Ref. 13 and (ii) a physically inconsistent behavior as a function of mass ratio $0 \leq \mu/M \leq 1/4$ (see M. Combescot in Ref. 27). Moreover in Refs. 34 and 35 it was introduced also an extrinsic dead layer in order to cure the first inconsistency but not the second one. In the present paper a different choice, that does not show neither of these inconsistencies, is suggested.

[29] H. Ishihara and K. Cho, Phys. Rev. B **41**, 1424 (1990).

[30] A. D'Andrea and D. Schiumarini, Eur. Phys. J. B **54**, 87 (2006).

[31] R. Atanasov, F. Bassani, A. D'Andrea, and N. Tomassini, Phys. Rev. B **50**, 14381 (1994).

[32] M. M. Glazov, H. Ouerdane, L. Pilozzi, G. Malpuech, A. V. Kavokin, and A. D'Andrea, Phys. Rev. B **80**, 155306 (2009).

[33] H. C. Schneider, F. Jahnke, S. W. Koch, J. Tignon, T. Hasche, and D. S. Chemla, Phys. Rev. B **63**, 045202 (2001); see also J. Tignon, T. Hasche, D. S. Chemla, H. C. Schneider, F. Jahnke, and S. W. Koch, Phys. Rev. Lett. **84**, 3382 (2000).

[34] D. Viri, R. Del Sole, and A. D'Andrea, Phys. Rev. B **48**, 9110 (1993).

[35] D. Viri and R. DelSole, Phys. Rev. B **52**, 11891 (1995).

[36] S. Schumacher, G. Czycholl, and F. Jahnke, Phys. Status Solidi B **234**, 172 (2002).

[37] In order to perform very accurate variational minimization of the Wannier center-of-mass energy in a quantum well, we have used the equations given in Ref. 30, where all the indeterminate (0/0) quantities, present in the implicit equations of Ref. 25, were analytically eliminated in order to improve the numerical accuracy.

[38] V. M. Agranovich and V. L. Ginzburg, *Crystal Optics and Spatial Dispersion and Excitons* (Springer, New York, 1986).

[39] E. O. Kane, Phys. Rev. B **11**, 3850 (1975).